Characterization of Common Mode Chokes at High Frequencies With Simple Measurements

C. Domínguez-Palacios, J. Bernal, *Senior Member, IEEE*, and M. M. Prats, *Senior Member, IEEE*

***Abstract*—In this paper, we present a technique to characterize common mode chokes at high frequencies that only requires a measurement, which can be performed with a spectrum analyzer with the tracking generator. This technique is based upon a theoretical modal analysis of the common mode choke as a four-ports device. This analysis demonstrates that the transmission coefficient measured for one of the windings of the common mode choke, while the other winding is open circuited will always show two minimums, which are associated with resonances involving currents flowing, respectively, in common mode and in differential mode in the common mode choke. Therefore, the response at high frequencies of the common mode choke to both a common mode and a differential mode stimulus can be foreseen from the measurement of this transmission coefficient. Moreover, from the analytical expressions obtained for the frequencies of resonance of the common mode choke in that configuration, we develop a method for obtaining the capacitive, resistive, and inductive parameters of a circuit model of the common mode choke. To validate the proposed technique different commercial common mode chokes have been measured and the predicted performance of the model has been compared with measured responses. We have verified that in all the cases the measured transmission coefficient exhibits the resonant behavior predicted by the theoretical analysis. We have checked that in most cases the method designed for extracting the high-frequency parameters of the circuit model of the common mode choke yields an accurate model of the device up to frequencies as high as 30–50 MHz. An exception are common mode chokes made of materials with an extreme variation of their properties with regards to frequency, such as nanocrystalline materials.**

***Index Terms*—Circuit modeling, electromagnetic compatibility, electromagnetic interference, filtering.**

I. Introduction

CURRENT trends toward the increase of switching frequencies and power density of power converters make electromagnetic interference (EMI) problems an increasingly critical issue [1], [2]. In this context, proper design and characterization of EMI filters over a wide range of frequencies can greatly help to keep noise emissions under control, while at the same time preventing designed over-specification. This is specially important in applications where strict requirements of size and weight are combined with stringent electromagnetic compatibility (EMC) regulations, as for example in aero and avionics engineering [3].

Common mode chokes (CMC) are a key component of EMI filters intended mainly for common mode (CM) current suppression [2], [4], [5]. A CMC relies on the high inductance presented to CM currents by two magnetically coupled windings on a core made from materials with high permeability. High-frequency differential mode (DM) noise is also attenuated to some extent by the leakage inductance of the CMC [6]. These effects should be incorporated in the circuit model of the filter for predicting the conducted emission of the equipment and for improving the design of the filter. However, in practice the performance of a CMC is significantly undermined by parasitic effects at high frequencies [7]. In fact, a simple circuit model of the CMC-based solely upon inductive components typically exhibits very poor accuracy at frequencies above several hundreds of kilohertz up to a few megahertz [2]. Therefore, a method for obtaining an accurate model of the CMC that accounts for resistive and capacitive parasitics is of paramount importance for avoiding a time-consuming trial and error process in the design of an EMI filter.

In general, CMCs are difficult to characterize because a CMC is a device with four terminals whose response depends on the connection, the type of noise (CM or DM) flowing through it and the frequency-dependent permeability of the core material [8], [9]. Despite that, and due to the interesting nature of the problem, many different techniques have been reported in order to provide a model of a CMC, which can perform well at high frequencies. Most of these techniques require inputs such as windings, core geometries, and permeability of the core. From those data they calculate parasitic elements by using analytical expressions [10]–[12] or by solving a three-dimensional electromagnetic model of the CMC with numerical techniques [1], [13]. This makes these techniques very useful for CMC design. However, these techniques are not always easy to use for characterization and/or selection of those CMCs already available. This is due to the fact that for commercial CMCs construction data and other basic data, such as properties of the core, are seldom available from vendors or respective datasheets. Moreover, for some presentations of CMCs (for example sealed components and/or shielded filters) even basic data such as the number of turns and length of wire are difficult to ascertain. An alternative approach to characterize commercial CMCs is

Manuscript received March 8, 2017; revised May 22, 2017; accepted July 4, 2017. Date of publication July 19, 2017; date of current version February 1, 2018. This work was supported by the Spanish Ministerio de Economía y Competitividad under Project TEC2014-54097-R. Recommended for publication by Associate Editor F. COSTA. *(Corresponding author: J. Bernal.)*

C. Domínguez-Palacios and M. M. Prats are with the Department of Ingeniería Electrónica, Universidad de Sevilla 41092, Spain (e-mail: cardompal@alum.us.es; mmprats@us.es).

J. Bernal is with the Department of Física Aplicada III, Universidad de Sevilla 41092, Spain (e-mail: jbmendez@us.es).

Color versions of one or more of the figures in this paper are available online at http://ieeexplore.ieee.org.

Digital Object Identifier 10.1109/TPEL.2017.2724639

to model the CMC from measurements, as proposed in [14]–[17]. These techniques require the performance of impedance measurements of the CMC with different connection schemes. The curves obtained are then fitted to those of a corresponding physical or behavioral circuit. In general, these techniques can be used to characterize CMCs with very complex behaviors [17]. However, the measurement of impedances (magnitude and phase) require the use of sophisticated equipment such as vector network analyzers (VNAs) or impedance analyzers that have to be carefully calibrated to eliminate the effects of connectors and cables. Also, some decisions have to be taken in some cases on impedance curves and/or manual adjustments made to eliminate negative circuit elements and obtain valid solutions [16].

In this paper, we present a technique to extract the parasitic elements of a CMC from simple measurements that can be carried out with a spectrum analyzer (SA) with tracking generator (TG). By performing a modal analysis on a circuit model of the CMC that incorporates the parasitic elements, we study the physical significance of the frequencies of resonance, which appear when measuring the coefficient of transmission of one of the windings of the CMC, while the other is open circuit. We demonstrate that for this particular and simple-to-implement configuration of the CMC, the transmission coefficient always exhibits two minimums (zero in transmission in the ideal lossless case) which are related to the two frequencies of resonance of the CMC, respectively, corresponding to CM and DM excitations of the two windings of the CMC. This permits a quick and easy prediction of the performance of a given CMC or even a comparison of performances between several CMCs. This can be a great help to speed up the process of design or redesign of a practical EMI filter. Moreover, we show that the analytical expressions obtained for these frequencies of resonance allows for development of a simple approach to determine the parasitic elements of the CMC from the measured transmission coefficient of the said configuration of the CMC. The accuracy of the circuit model obtained by this technique is checked by comparing the predicted attenuation by the model of the CMC for CM and DM currents with measured attenuations. This comparison is performed here for a wide sample of different commercial CMCs to determine the effective scope of the method.

II. Analysis

Fig. 1 shows a lumped-element circuit model of a CMC. The model includes two equal magnetically coupled windings that determine the low-frequency response of the choke. Also, parasitic self-capacitances of windings (C_t) and capacitances between windings (C_w) have been added to account for the electrical couplings that determine the high-frequency behavior of the CMC [5], [11], [12]. In this model, losses within the magnetic material are accounted for by resistors (R_c) placed in parallel with the coupled inductors.

Usually CMCs are characterized by measuring their response to CM and DM excitations. This can be easily achieved by using an SA with TG, as shown in Fig. 2 [15]. In Fig. 2(a), it can be observed that connected in CM approximately equal currents are expected to enter at nodes 1 and 2, whereas equal currents

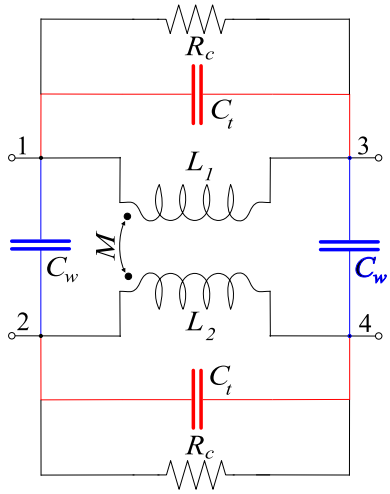

Fig. 1. Circuit model of a common mode choke (CMC).

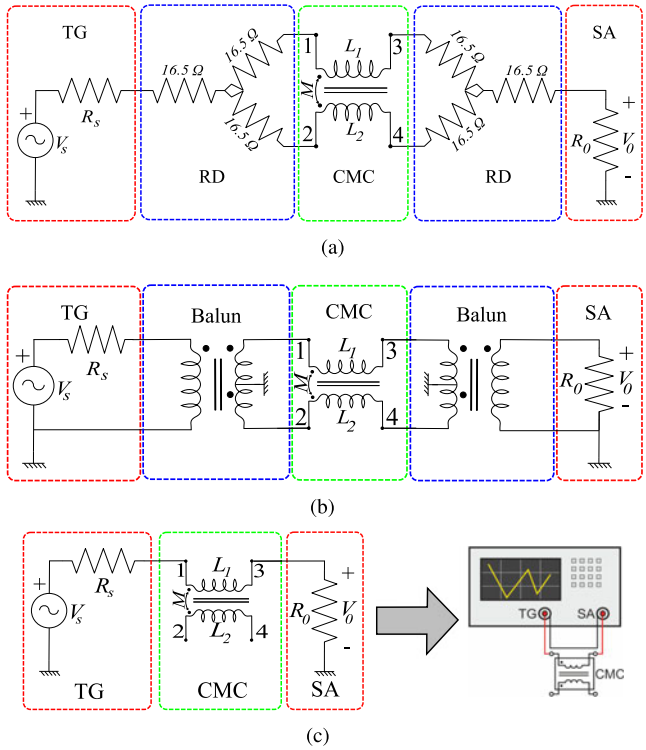

Fig. 2. Experimental setups for measuring a CMC with a spectrum analyzer (SA) with tracking generator (TG). (a) Common mode (CM) setup. (b) Differential mode (DM) setup. (c) Open-circuit mode (OC) setup.

with phases at +180 are expected to flow through these nodes when the CMC is excited in the DM configuration of Fig. 2(b). The purpose of the resistive dispatchers (RD) present in the CM setup is to avoid impedance discontinuity caused by the splitting lines. Fig. 2(c) shows an alternative setup where one of the windings of the CMC is connected between the TG and the SA whereas the other winding is left open circuit (OC). We will refer to this configuration as open circuit. Note that the OC setup does not require the use of the high-frequency baluns (transformers) or RD that are necessary for the CM and DM connections. However, in this connection the CMC is driven

simultaneously in both CM and DM. Therefore, at first glance the OC setup does not seem as useful as the other connections for the study and characterization of a CMC.

The connections shown in Fig. 2 allow the measuring of the magnitude of the transmission coefficient, S_{21}, in respect to frequency. To analyze the effect at different frequencies of each parameter of the circuit model of Fig. 1 in the response of the CMC for each configuration in Fig. 2 and also to determine the impact of these parameters on the frequencies of resonance that appear in each setup it would be useful to obtain analytical expressions for S_{21} in each case.

In general, symmetric two-port networks, such as CMCs, admit an analysis based upon decomposition on even (CM) and odd (DM) responses. The response to a general excitation can then be calculated by using the superposition principle. However, this convenient analysis cannot be straightforwardly applied here due to the presence of parasitic capacitances. It should be noted that for the CM setup of Fig. 2(a), under the criteria that currents entering a node are positive, we can assume that $I_1 = -I_3$ and $I_4 = -I_2$ and, therefore, the two pairs of terminals 1–3 and 2–4 can be regarded as the two ports of the symmetric network [18]. On the contrary, in the DM configuration [see Fig. 2(b)] nodes 1–3 and 2–4 do not satisfy the port condition at high frequencies, since the effect of the capacitors C_w is not negligible. Therefore, a simple two-ports model cannot be used to analyze the response of the CMC for all the configurations of interest over a wide range of frequencies. To overcome this difficulty, in this section we instead propose an analysis that treats the CMC as a four-ports network and that decomposes any excitation at the four ports of the CMC in four modes that are the eigenvectors that diagonalize the admittance matrix of the system. This formulation will permit the obtaining of closed-form expressions for $S_{21}(\omega)$ for any configuration of a CMC modeled with a reciprocal and symmetrical circuit as that in Fig. 1.

When considered as a four-ports network, the circuit in Fig. 1 can be characterized by an admittance matrix that relates currents and voltages (referred to ground) in the four ports

$$\begin{pmatrix} I_1 \\ I_2 \\ I_3 \\ I_4 \end{pmatrix} = \begin{pmatrix} Y_{11} & Y_{12} & Y_{13} & Y_{14} \\ Y_{12} & Y_{11} & Y_{14} & Y_{13} \\ Y_{13} & Y_{14} & Y_{11} & Y_{12} \\ Y_{14} & Y_{13} & Y_{12} & Y_{11} \end{pmatrix} \begin{pmatrix} V_1 \\ V_2 \\ V_3 \\ V_4 \end{pmatrix}. \tag{1}$$

Where symmetry considerations allow us to assume that $Y_{12} = Y_{34}$, $Y_{13} = Y_{24}$, and $Y_{14} = Y_{23}$. The eigenvectors of the matrix $[Y]$ are $[V]$ excitations (modes) that create equal current responses in the four nodes of the circuit (i.e., that diagonalize the matrix). The constant of proportionality between currents and voltages for each mode is the eigenvector (admittance) of that particular eigenvalue (mode). In this highly-symmetrical case the four eigenvalues of $[Y]$ can be identified by simple inspection. A general voltage excitation can then be expressed as the sum of four eigenvectors or modes in the following form:

$$\begin{pmatrix} V_1 \\ V_2 \\ V_3 \\ V_4 \end{pmatrix} = V_{\mathrm{C}} \begin{pmatrix} 1 \\ 1 \\ 1 \\ 1 \end{pmatrix} + V_{\mathrm{V}} \begin{pmatrix} 1 \\ -1 \\ 1 \\ -1 \end{pmatrix} + V_{\mathrm{H}} \begin{pmatrix} 1 \\ 1 \\ -1 \\ -1 \end{pmatrix} + V_{\mathrm{D}} \begin{pmatrix} 1 \\ -1 \\ -1 \\ 1 \end{pmatrix}. \tag{2}$$

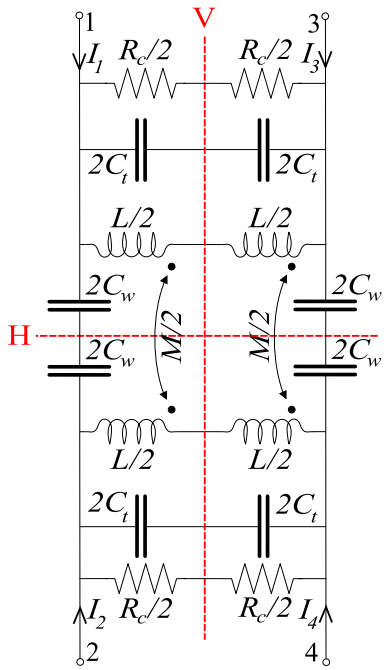

Fig. 3. Circuit model of the common mode choke equivalent to that of Fig. 1 but modified to explicitly show the planes of symmetry *V* and *H*.

The system of linear equations posed by (2) allows us to calculate the amplitudes of these four modes for a general excitation at the four ports of the CMC

$$V_{\mathrm{C}} = \frac{1}{4}(V_1 + V_2 + V_3 + V_4) \tag{3}$$

$$V_{\mathrm{V}} = \frac{1}{4}(V_1 - V_2 + V_3 - V_4) \tag{4}$$

$$V_{\mathrm{H}} = \frac{1}{4}(V_1 + V_2 - V_3 - V_4) \tag{5}$$

$$V_{\mathrm{D}} = \frac{1}{4}(V_1 - V_2 - V_3 + V_4). \tag{6}$$

These four modes allow us to express any excitation as a sum of its C, H, V, and D components, and the response of the system can be expressed in terms of the admittances of these modes. The next step of our analysis is to calculate the admittances of these four modes.

To calculate the admittances of the four modes in (2) it is useful to note that these modes represent different combinations of even and odd excitations with respect to two perpendicular planes of symmetry that can be depicted in the circuit of the CMC in Fig. 1. These planes of symmetry are referred to as horizontal (*H*) and vertical (*V*) planes and they are represented in Fig. 3. Note that in this figure the elements of the circuit model has been split into two elements connected in series to identify the planes of symmetry. For each mode, the *H* and *V* planes in Fig. 3 can be considered as either a magnetic wall (open circuit) or an electric wall (ground). Therefore, each mode has a very simple equivalent circuit from which the admittance of

TABLE I
EQUIVALENT CIRCUITS AND ADMITTANCES OF THE FOUR MODES OF THE CMC TREATED AS A FOUR-PORTS DEVICE

Mode	H Plane	V Plane	Circuit	Admittance
C	magnetic	magnetic	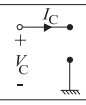	$Y_{\mathrm{C}} = 0$
V	electric	magnetic	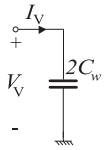	$Y_{\mathrm{V}} = j\omega 2C_w$
H	magnetic	electric	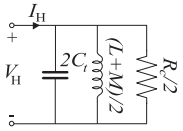	$Y_{\mathrm{H}} = 2\left(j\omega C_t + \frac{1}{j\omega(L+M)} + \frac{1}{R_C}\right)$
D	electric	electric	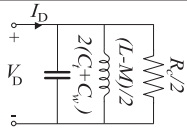	$Y_{\mathrm{D}} = 2\left(j\omega(C_t + C_w) + \frac{1}{j\omega(L-M)} + \frac{1}{R_C}\right)$

the mode can be obtained. The equivalent circuit of each mode along with the calculated admittances are represented in Table I. As shown in that table, for mode C we have $Y_{\mathrm{C}} = 0$. However, it must be pointed out that in practice at each terminal of the CMC there may be a parasitic capacitance to ground that we have disregarded. This is a reasonable approximation validated by the results shown in Section IV. This approximation is expected to remain valid as long as strong electric coupling of the CMC to nearby grounded conductors is avoided when performing measurements of the CMC in the different configurations of Fig. 2.

Once the admittances of the four modes are known, the $S_{21}(\omega)$ coefficient for each configuration of Fig. 2 can be most easily calculated by identifying the modes that are excited in each particular connection of the CMC. The formula obtained for $S_{21}(\omega)$ will allow us to calculate the frequencies of resonance expected for the CM, DM, and OC connections in terms of the parameters of the circuits that model the CMC. To simplify the calculation of the frequencies of resonance, we will assume a lossless case ($R_c = \infty$). Also, resistances R_s and R_0 in Fig. 2 are taken to be equal: $R_s = R_0 = R = 50\ \Omega$, which is commonly true.

A. Connected in CM

The CM connection of Fig. 2(a) introduces a magnetic wall boundary condition along the plane of symmetry *H* of the CMC (see Fig. 3). With this condition, Table I shows that only C and H modes can be excited. However, since we are disregarding parasitic capacitance to ground, $Y_{\mathrm{C}} = 0$, only currents that are associated to the H mode appear. These currents flow horizontally in the scheme of Fig. 3, hence the H name for this mode. The S_{21} coefficient can, therefore, be expressed as

$$S_{21}^{\mathrm{CM}} = \frac{2RY_{\mathrm{H}}}{2RY_{\mathrm{H}} + 1}. \tag{7}$$

For the lossless case the transmission coefficient of (7) gives zero at a frequency such that $Y_{\mathrm{H}} = 0$. This leads to the following equation for this frequency of resonance:

$$\omega_{\mathrm{CM}} = \frac{1}{\sqrt{C_t(L+M)}}. \tag{8}$$

In the general lossy case this resonance will lead to $Y_{\mathrm{H}} = 2/R_c$ and a minimum for $|S_{21}^{\mathrm{CM}}|$.

Summing up, the CM configuration excites the H mode, which forces currents to flow in CM through the CMC. This causes the equivalent inductance of each winding to be $L + M$. At ω_{CM} this inductance resonates with the self-capacitance of the windings C_t, which results in a minimum of transmission in the CM configuration.

B. Connected in DM

The DM connection shown in Fig. 2(b) forces an electric wall condition on the *H* plane of symmetry of the CMC. This condition rules out C and H modes, allowing only V and D modes to exist. The S_{21} coefficient for this connection can then be obtained by using the superposition principle and can be expressed as

$$S_{21}^{\mathrm{DM}} = \frac{RY_{\mathrm{D}}}{RY_{\mathrm{D}} + 2} - \frac{RY_{\mathrm{V}}}{RY_{\mathrm{V}} + 2}. \tag{9}$$

From (9), it is clear that in the lossless case $S_{21}^{\mathrm{DM}} = 0$ requires $Y_{\mathrm{V}} = Y_{\mathrm{D}}$. From the expressions of the mode admittances in Table I it follows that this zero condition will be satisfied at the following frequency:

$$\omega_{\mathrm{DM}} = \frac{1}{\sqrt{C_t(L-M)}}. \tag{10}$$

Therefore, the DM excitation excites the D mode, which is the only mode that forces DM currents to flow in the CMC. This causes the equivalent inductance of each winding to be

$L - M$. However, note that due to the existence of C_w, a V mode is also excited. Equation (9) shows that this V mode causes the transmission coefficient to decrease. It also modifies the resonance condition from $Y_{\rm D} = 0$ to $Y_{\rm D} = Y_{\rm V}$. This removes the contribution of the capacitances C_w to this resonance, thus slightly increasing the frequency of resonance for the DM setup above that of the D mode alone.

C. Connected in OC

The condition for the OC connection [see Fig. 2(c)] is $I_2 = I_4 = 0$. It can be demonstrated that this condition can be satisfied only if modes H and D are excited by the same current $|I_{\rm D}| = |I_{\rm H}|$, whereas mode V is not excited. This means that for the OC configuration the CMC is driven simultaneously in CM (H mode) and in DM (corresponding to the D mode), both with the same current which is equal to one half of the current that enters terminal 1 (and leaves terminal 3). In fact, from (2) it can be seen that $V_1 - V_3 = 2(V_{\rm H} + V_{\rm D})$. This means that the D and the H modes can be considered as connected in series, presenting a net admittance

$$Y_{\rm OC} = \frac{Y_{\rm H} Y_{\rm D}}{Y_{\rm D} + Y_{\rm H}}. \tag{11}$$

Consequently, the S_{21} coefficient measured with this arrangement can be expressed as

$$S_{21}^{\rm OC} = \frac{2RY_{\rm OC}}{2RY_{\rm OC} + 1}. \tag{12}$$

This equation reveals that when the CMC is connected in the OC configuration the S_{21} curve should exhibit two zeros (or minimums in a lossy case): the first zero at a lower frequency which corresponds to $Y_{\rm H} = 0$ and the second one at a higher frequency that corresponds to the condition $Y_{\rm D} = 0$. These two frequencies of resonance are

$$\omega_{\rm OC1} = \frac{1}{\sqrt{C_t(L+M)}} = \omega_{\rm CM} \tag{13}$$

$$\omega_{\rm OC2} = \frac{1}{\sqrt{(C_t + C_w)(L-M)}} < \omega_{\rm DM}. \tag{14}$$

Physically this means that the CMC excited in the OC configuration resonates with currents flowing in CM (inductance $L + M$ in parallel with C_t) at a lower frequency given by (13). It also resonates at the higher frequency (14) with currents flowing in DM (inductance $L - M$ in parallel with $C_t + C_w$).

The relationship between the response of the CMC in the OC configuration and its response to CM and DM currents can be illustrated with an example. With this aim in Fig. 4, we represent the magnitude and phase of S_{21} measured for an actual CMC, described in the caption. We represent results for the three configurations (CM, DM, and OC) of Fig. 2. From Fig. 4, it can be observed that the output of the CM and OC configurations are similar at low frequencies both in magnitude and phase. This can be understood because at low frequencies $Y_{\rm D} \approx 2/j\omega(L-M) \gg Y_{\rm H} \approx 2/j\omega(L+M)$ and consequently from (11) $Y_{\rm OC} \approx Y_{\rm H}$. Therefore, $S_{21}^{\rm OC}$ in (12) becomes similar to $S_{21}^{\rm CM} \approx 2RY_H$ (7). In other words, although in the OC configuration both a D mode and an H mode are excited with the same current, at low frequencies the output voltage is dominated by that corresponding to the H mode (CM currents in the CMC) because the admittance of this mode is much lower. The first minimum of the OC curve in Fig. 4(a) is, therefore, the resonance of the H mode, and coincides with that of the CM curve. After this first minimum Y_H becomes capacitive (phase 90°) and its magnitude increases with frequency, whereas Y_D remains inductive and decreases with frequency (with phase $-$ 90°). When the magnitudes of these two impedance become equal resonance occurs and ideally $|S_{21}^{\rm OC}| = 1$. This corresponds to the maximum that can be observed in the OC curve in Fig. 4(a) at approximately 1 MHz. Note that at this maximum the CMC behaves as a short circuit and, therefore, the phase of $S_{21}^{\rm OC}$ is zero (i.e., resistive). After this peak of the OC curve Y_D that is associated with DM currents flowing through the CMC, becomes dominant in (12), and the phase of the OC curve becomes inductive again. At higher frequencies the OC curve presents a second minimum. This second minimum corresponds to the frequency of resonance of the D mode (14) and results in another change

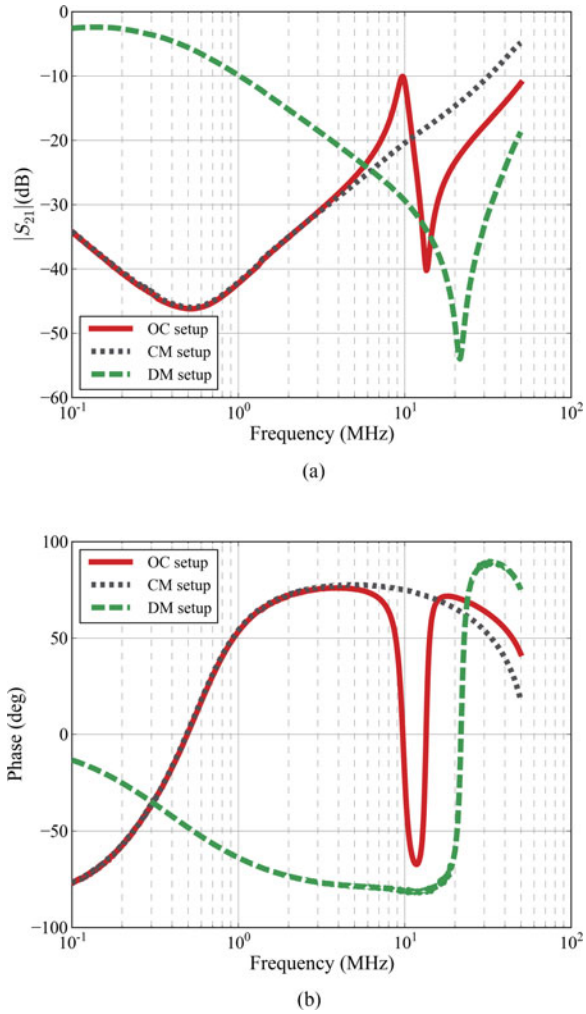

Fig. 4. Magnitude an phase of S_{21} for the CMC Würth Elecktronik 7446121007 (6.8 mH), listed in Table II and in Table III, when measured using the three configurations of Fig. 2. (a) Magnitude. (b) Phase.

from an inductive to a capacitive phase in the corresponding curve of Fig. 4(b), as expected. Note that this resonance occurs at a frequency slightly lower than that of the DM configuration. As explained in our previous analysis, this is associated with the fact that in the DM configuration the V mode is excited along with the desired D mode, and this results in a slight increase of the frequency of resonance of the DM setup (10) due to the influence of the parasitic capacitances C_w. Finally, note that at sufficiently high frequencies the already capacitive admittances shown by the CMC in the different configurations become so high that the corresponding S_{21} coefficients are progressively dominated by the source and load impedances of the circuit, which are resistive.

Summing up, the OC response of a CMC is dominated by the CM response of the CMC at low frequencies and by the DM response at high frequencies, in such a way that the transmission coefficient for the OC connection of the CMC presents two frequencies of resonance (minimums of transmission) associated, respectively, with CM and DM excitations of the CMC. This implies that measurements in a simple OC setup, which does not require auxiliary circuits as baluns or RD, can provide very valuable information about the behavior of the CMC with respect to CM and DM noise at different frequencies. Moreover, because closed-form expressions have been obtained for the frequencies of resonance of the CMC (13–14), the measured frequencies of resonance can be used to calculate the parameters of the high-frequency model of the CMC, as described in Section III.

Interestingly, the fact that the effect of the coupling between two *L–C* rings is to split the frequency of resonance of each one of the rings into two frequencies of resonance associated with the so-called even and odd excitations of the inductors (corresponding to CM and DM excitations of the CMC) has been well studied in the field of the design of RF/microwave narrow-band bandpass filters [19]. In this sense, the pair of coupled windings that make up a CMC can be regarded at sufficiently high frequency as a pair of synchronously tuned coupled-resonator circuits presenting both electric and magnetic coupling between them. However, because of the particular way in which those resonant rings are excited in microwave filters the theory of synchronously tuned coupled-resonator circuits has been developed by considering a pair of coupled *L–C* rings as a two-ports device. In contrast, the four-ports formulation presented here for CMCs allows us to deal with the particularities of the configurations in Fig. 2. For example, as we have seen, this formulation helps to explain the difference between the frequencies of resonance measured in the DM and OC connections of the CMC.

III. Description of the Method

The analysis expounded in the previous section relates the excitation of a CMC using the CM, DM, and OC configurations of Fig. 2 with the excitation of the four modes of a symmetrical four-ports network. That analysis shows that the admittances of modes D and H correspond to two similar but separate parallel *RLC* circuits and that these admittances are excited in series in the OC configuration, whereas D mode is not excited in the CM setup and H mode is not excited in the DM setup. Based upon this analysis, Fig. 5 shows an alternative and equivalent model of the CMC that explicitly shows the contribution of the admittances of the modes H and D by separating the model of the CMC in two different blocks. Each block includes two coupled inductances with opposite ideal coupling coefficients ($+1$ and -1). The block with $k = 1$ (CM block in Fig. 5) is short-circuited by DM currents whereas the block with $k = -1$ (referred to as DM block) is short-circuited by CM currents. This alternative model is in principle equivalent to that of Fig. 1 but it presents several advantages. First, it explicitly shows the parameters that affect CM and DM currents in the CMC. For instance, it shows that the capacitances C_w have no effect on CM currents and that $L + M$ affects CM currents but the inductance acting against DM currents is $L - M$. Also, the model in Fig. 5 makes it easier to understand the response of the CMC when excited in the OC configuration as the response of the connection of two *LCR* blocks (CM and DM blocks) in series. An additional advantage of the use of two separate blocks to model the CMC is that it makes it easier to take into account the frequency-dependent behavior of the inductive and resistive parameters of the CMC [5], [8] in the model. In fact, note that this model allows us to assign different values to the parallel resistances in each block. This way $R_{\rm CM}$ in Fig. 5 accounts for the lossy behavior of the CMC at the (low-frequency) CM resonance and $R_{\rm DM}$ accounts for the lossy behavior of the CMC at the (high-frequency) DM resonance. Additionally, the circuit in Fig. 5 suggest that, since the inductance of the choke is expected to vary with frequency, it would be a better strategy to treat $L + M$ and $L - M$ as two separate and independent parameters in instead of looking for a mutual coupling M between the inductances L valid throughout the frequency range.

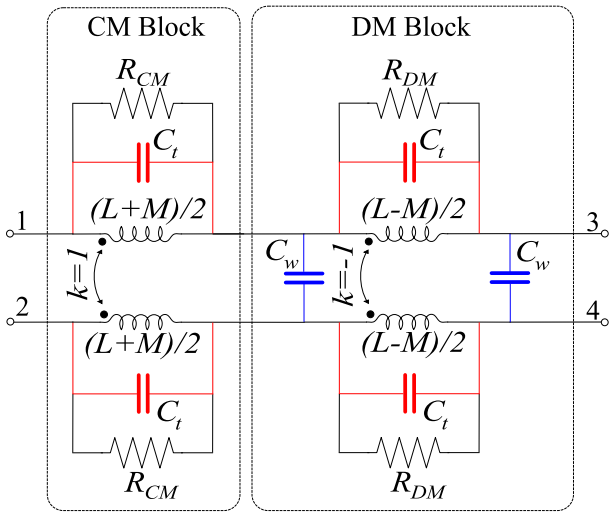

Fig. 5. Equivalent circuit model of a CMC with CM and DM blocks.

It should be pointed out that a similar model based on CM and DM blocks is also proposed in [17] as a behavioral model for CMCs, although only inductive parameters are separated in the blocks used in [17]. The theoretical analysis presented in Section II explains the good performance of the behavioral

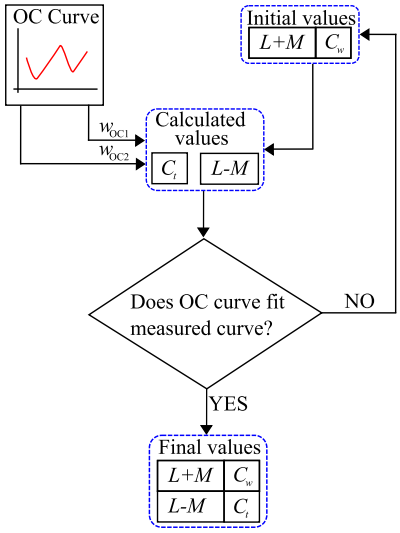

Fig. 6. Scheme of the proposed method for calculating the parameters of the model of the CMC.

model proposed in that work. However, note that in this paper the circuit elements have a physical interpretation. Also, and in accordance with that, our method makes use of an entirely different approach, based on simpler measurements, to obtain the parameters of the model, as will be seen.

The enhanced model of the CMC represented in Fig. 5 along with the analytical expressions obtained for the frequencies of resonance of the CMC in the OC configuration (13, 14) make it possible to design a method to obtain the parasitic elements that determine the high-frequency response of the CMC exclusively from $|S_{21}^{\mathrm{OC}}|$ as measured.

First, the resistances R_{CM} and R_{DM} in Fig. 5 can be obtained from the magnitude of $S_{21}^{\mathrm{OC}}(\omega)$ measured at the two frequencies of resonance $\omega_{\mathrm{OC}1}$ and $\omega_{\mathrm{OC}2}$ as

$$R_{\mathrm{CM}} \approx 4R \times 10^{|S_{21}^{\mathrm{OC}}(\omega_{\mathrm{OC}1})|/20} \tag{15}$$

$$R_{\mathrm{DM}} \approx 4R \times 10^{|S_{21}^{\mathrm{OC}}(\omega_{\mathrm{OC}2})|/20} \tag{16}$$

where the magnitudes of S_{21} are expressed in decibels and $R_{\mathrm{CM}}, R_{\mathrm{DM}} \gg R = 50\ \Omega$ is assumed (which is true in most practical cases).

The rest of the parameters of the model in Fig. 5, namely $L + M$, $L - M$, C_t, and C_w can be obtained in an iterative process whose flowchart is shown in Fig. 6. In that approach, the initial values of $L + M$ and C_w have to be provided. The inductance $L + M$ can be approximated as two times the inductance of the windings, which can usually be found on the datasheet of the CMC. The value of C_w is usually in the order of a few picofarads, therefore any value in that order of magnitude can be postulated as initial value. The capacitance C_t can be calculated from $L + M$ and $\omega_{\mathrm{OC}1}$ by using (13). Then, $L - M$ can be obtained from C_w, C_t and $\omega_{\mathrm{OC}2}$ by using (14). Once the parameters have been calculated, the estimated OC curve over the range of frequencies measured can be readily obtained using (12) and the expressions for Y_{H} and Y_{D} provided in Table I. Then, a curve-fitting algorithm [20] can be used to iterate the process and find the set of parameters that best fit the measured OC curve. Once a final set of parameters is found, the CM and DM responses of the CMC can be predicted by using (7) and (9) with the modal admittances in Table I. An interesting feature of this method is that all the calculations are performed by using analytical expressions. As a consequence the curve-fitting process is quite fast, with typical calculation times below 1 s.

It is worth pointing out that, in principle, the curve-fitting algorithm could be designed in such a way that all the four parameters $L - M$, $L + M$, C_w, and C_t are treated as input parameters and, therefore, the OC curve can be fitted without enforcing a particular relationship between them. However, by forcing (13) and (14) the physical role of the parameters is preserved, hence avoiding results that imply negative elements which can cause simulation problems [16].

Another interesting characteristic of the approach described in Fig. 5 is that it allows us to obtain the model of the CMC exclusively from the measurement of the the OC curve. Alternatively, if an *LCR* meter is available it is also possible to obtain $L + M$ from the measurement at low frequency of the input inductance of one winding with the secondary winding being open circuit (which yields L), which provides $L(1 - k^2) \approx 2(L - M)$. Also C_w can be estimated by directly measuring the capacitance between the windings, i.e., between the even and the odd terminals in Fig. 1, which is $2C_w$. With these input parameters and the magnitude of the S_{21}^{OC} coefficient at the two frequencies of resonance, $\omega_{\mathrm{OC}1}$ and $\omega_{\mathrm{OC}2}$, it is possible to calculate the rest of the parameters R_1, R_2, C_t, and $L - M$ following the steps explained above. This alternative approach dispenses with the curve fitting process and works well in many cases. However, it requires additional (although simple) measurements and suffers from a lack of adaptability and flexibility when compared with the previously described iterative procedure. This can be a serious drawback when dealing with some CMCs exhibiting a significant dependence on the frequency of their inductive parameters, as we will see in Section IV.

As a final remark, it must be highlighted that in the method described in this section the leakage inductance of the CMC ($L - M$) is calculated from the resonance at the higher frequency ($\omega_{\mathrm{OC}2}$) of the OC curve. Although in principle, $L - M$ could also be estimated from the inductance measurements performed with the *LCR* meter. However, an *LCR* meter typically measures at relatively low frequencies (between 15 and 200 kHz for the particular *LCR* meter used in this paper).[1] Due to the variation of the inductance with the frequency shown by most CMCs this may lead to significant errors in the estimation of $L - M$ at high frequencies. By calculating $L - M$ from $\omega_{\mathrm{OC}2}$ we estimate the impact of $L - M$ in the attenuation exhibited by the CMC at high frequencies, that is precisely where this effect is most noticeable.

IV. Results

As a first step to validate our analysis, we checked that commercial CMCs measured in the OC configuration in Fig. 2(c)

[1] Atlas *LCR*40 model from Peak Electronic Design Ltd.

TABLE II
CMCs Analyzed in This Paper in Order of Increasing Inductance

Manufacturer	Part number	Inductance (mH)
SCHAFFNER	RN112-4-02	0.7
TDK	B82722A2302N001	1.2
TDK	B82725A2103N001	1.8
TDK	B82726S2163N030	2.0
KEMET	SC-02-30G	3.0
SCHAFFNER	RN102-1-02	3.0
SCHAFFNER	RN102-0.6-02-4M4	4.4
WÜRTH ELEKTRONIK	7446121007	6.8
WÜRTH ELEKTRONIK	7448011008	8.0
EMIKON	FHE - 05 - 1055	10
WÜRTH ELEKTRONIK	744866103	10
WÜRTH ELEKTRONIK	7446631010	10
KEMET	SCF20 - 05 - 1100	11
SCHAFFNER	RN102-0.3-02-12M	12
KEMET	SU9V-R01180	18
MURATA	PLA10AN2230R4D2	22
SCHAFFNER	RN102-0.3-02-22M	22
WÜRTH ELEKTRONIK	7446630047	47

exhibit the resonant behavior as predicted by the modal analysis of Section II. We measured a range of CMCs from various manufacturers and with different inductances (listed in Table II) and we have found no exceptions to that behavior. A typical example of this is shown in Fig. 4. Although additional resonances can be observed in a few cases when approaching frequencies in the order of 100 MHz [17], the CM and DM resonances always appear below 30–50 MHz.

It must also be checked whether in general our approach is able to provide an useful circuit model of a CMC in a sufficiently broad frequency range. To do that, we have measured a broad sample of different CMCs. The list of Table II lists CMCs from different manufacturers covering a broad range of nominal inductances and with cores made up of different materials (iron powder, ferrite, and nanocrystalline). For these commercial CMCs, we have obtained the high-frequency parameters from $|S_{21}^{\mathrm{OC}}|$ measured in the OC configuration of Fig. 2(c) (OC curves) following the procedure described in Section III. Then, to study the usefulness of the circuit model obtained for the CMC, we have compared the actual performance of the CMCs when measured in the CM and DM setups of Fig. 2(a) and (b) with the responses predicted by the model of the CMC of Fig. 5 for these configurations. All the $|S_{21}|$ curves have been measured with a Rhode&Schwarz ZND VNA[2] over a frequency range (100 KHz–30 MHz) that covers the range of measurement for conducted emissions in many regulations [21]–[23].

Following the strategy of validation mentioned above, we have obtained good results in most cases. As an example, Fig. 7 compares measured and calculated $|S_{21}|$ curves for the KEMET SC-02-30G CMC (3 mH) listed in Table III. Note that the OC curve at low frequencies coincides with the CM curve, as expected from the explanation provided in Section III. Moreover, both curves and also the DM curve are well approximated by

[2]Note that since only magnitudes of S_{21} are needed, a spectrum analyzer can be used to the same end.

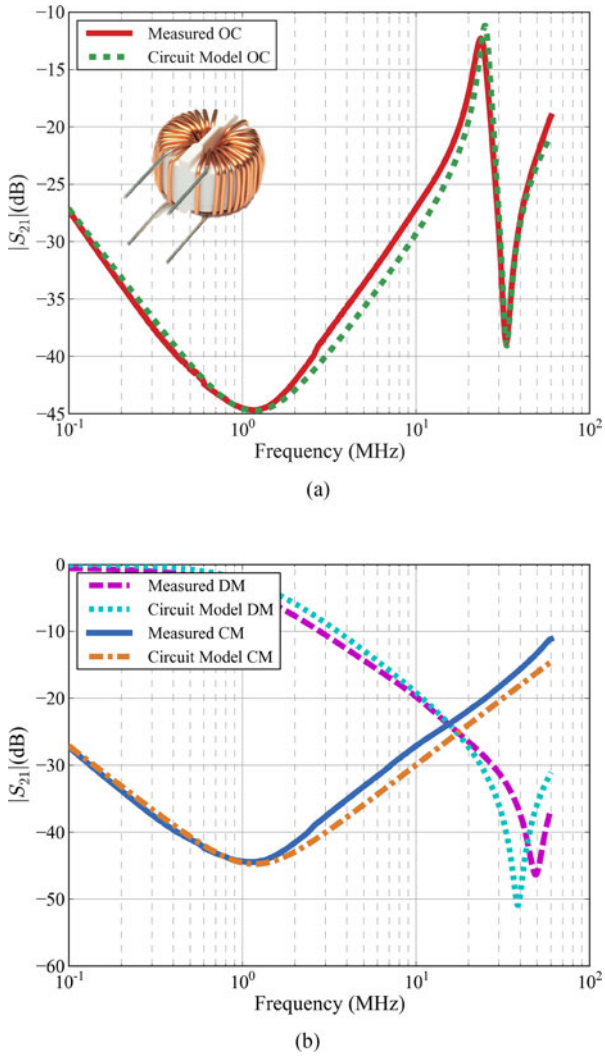

Fig. 7. Measured and approximated $|S_{21}|$ curves for the CMC shown in the upper figure and listed as KEMET SC-02-30G (3mH) in Table III. (a) Open Circuit (OC). (b) Common mode (CM) and differential mode (DM).

the high-frequency model with the parameters provided by our method, that are given in Table III.

As another example, Fig. 8 shows results for a sealed CMC of almost 7 mH (WÜRTH ELEKTRONIK 7446121007 in Table III). This CMC has slightly lower frequencies of resonance, and once again both the CM and the DM curves are correctly approximated up to frequencies in the order of a few tens of MHz by the high-frequency model of Fig. 5 with the parameters obtained by our method, which are shown in Table III.

A CMC with different construction (sectional windings) is analyzed in Fig. 9. This corresponds to the CMC listed as KEMET SU9V-R01180 in Table III. A good agreement can be observed in Fig. 9 between measured results and curves calculated with the parameters obtained from the OC curve of the CMC. Note that in this case the intrawinding capacitance C_t provided by our method (shown in Table III) is higher than those of the previous CMCs. This is probably due to the multilayer windings used in that CMC. This high C_t, along with the higher inductance of the CMC, accounts for the relatively low frequencies

TABLE III
DESCRIPTION AND PARAMETERS EXTRACTED FROM CMCS CHARACTERIZED IN THIS PAPER

Manufacturer and part number	L (mH) Datasheet	$L+M$ (mH)	$L-M$ (uH)	C_w (pF)	C_t (pF)	R_1 (kΩ)	R_2 (kΩ)
KEMET SC-02-30G	3	7.19	6.69	0.90	2.54	34.3	17.5
WÜRTH ELEKTRONIK 7446121007	6.8	16.9	12.8	5.35	5.56	40.9	20.6
KEMET SU9V-R01180	18	63.4	167	1.20	13.0	273	42.3
MURATA PLA10AN2230R4D2B	22	72.2	192	0.16	3.40	759	59.2
WÜRTH ELEKTRONIK 7448011008	8	3.47	8.75	0.27	1.76	23.9	11.2

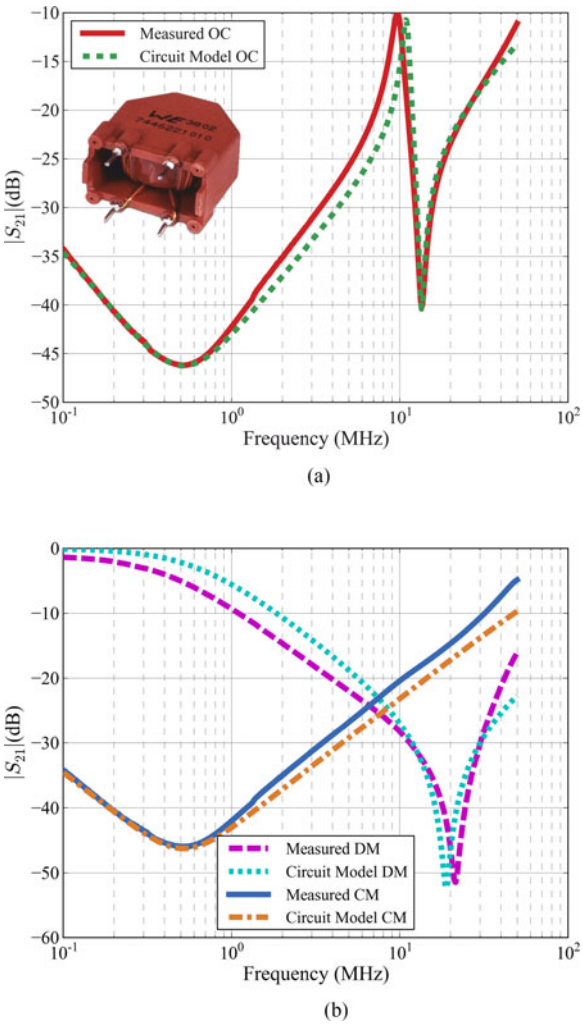

Fig. 8. Measured and approximated $|S_{21}|$ curves for the CMC shown in the upper figure and listed as WÜRTH ELEKTRONIK 7446121007 (6.8 mH) in Table III. (a) Open circuit (OC). (b) Common mode (CM) and differential mode (DM).

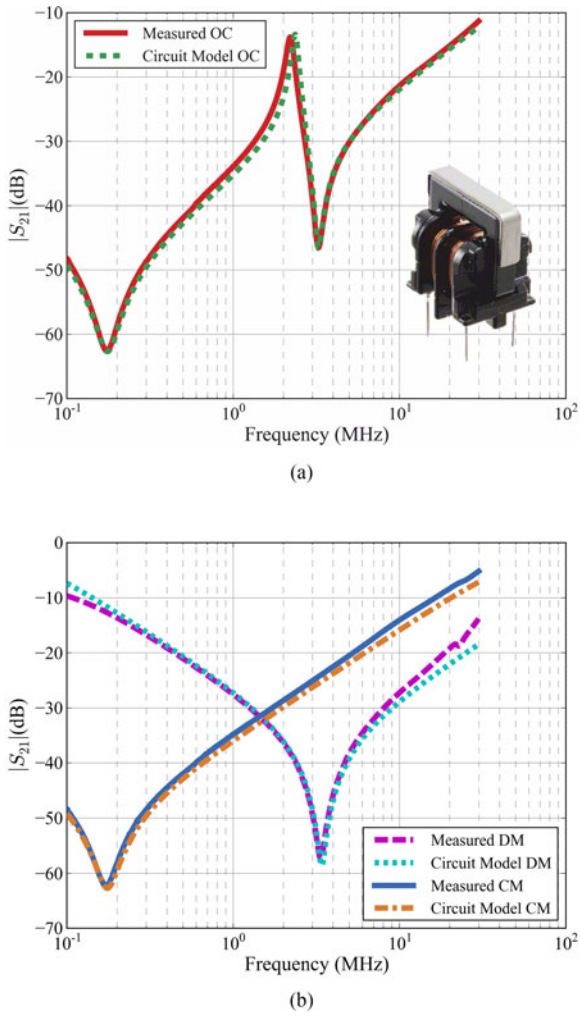

Fig. 9. Measured and approximated $|S_{21}|$ curves for the CMC shown in the upper figure and listed as KEMET SU9V-R01180 (18 mH) in Table III. (a) Open circuit (OC). (b) Common mode (CM) and differential mode (DM).

of resonance of this CMC. In fact, note that, taking into account that $L+M \approx 2L$, the $L+M = 63.4$ mH CM inductance obtained for this CMC corresponds to an L much higher than the value of 18 mH (measured at 1 kHz) specified in the datasheet. This example emphasizes the importance of an adequate characterization to estimate the actual response of CMCs at high frequencies.

The example discussed above illustrate the fact that, in general, the permeability of the core of most CMCs varies with frequency, resulting in a change of the inductances and resistances required to model the CMC. However, note that the response of the CMC to the CM excitation above the frequency of resonance of the CM, ω_{CM}, is dominated by the intrawinding capacitances C_t. Therefore, a change in the inductance of the CMC has no effect in the CM curve above that frequency. The same effect occurs for the DM curve. However, since the DM resonance occurs at much higher frequencies ($\omega_{DM} \gg \omega_{CM}$), the DM curve is strongly influenced by the inductance of the core in a much wider range of frequencies and, consequently,

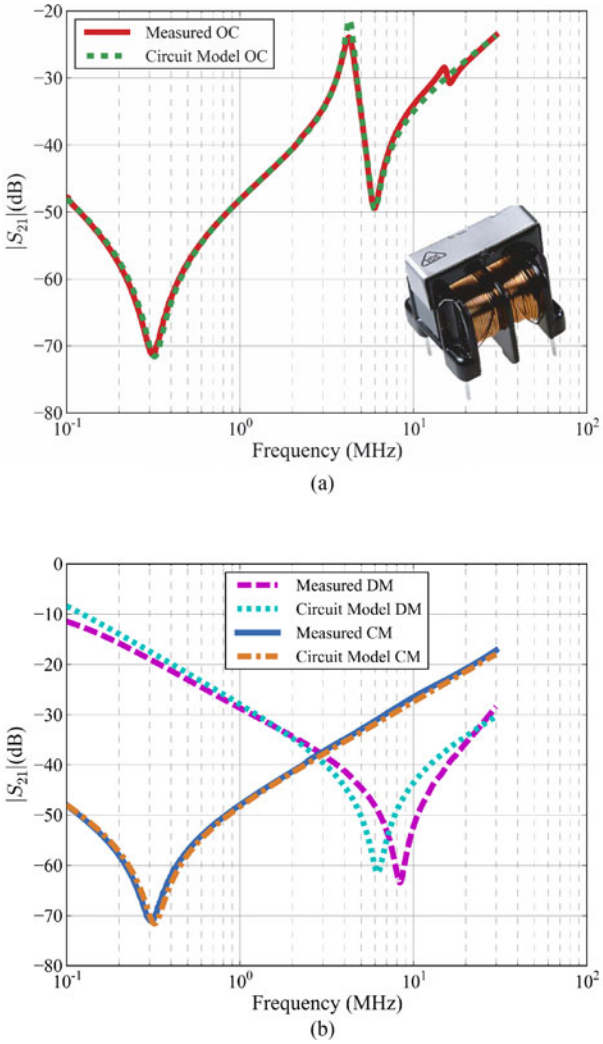

Fig. 10. Measured and approximated $|S_{21}|$ curves for the CMC shown in the upper figure and listed as MURATA PLA10AN2230R4D2B (22 mH) in Table III. (a) Open circuit (OC). (b) Common mode (CM) and differential mode (DM).

the DM curve is in general much more difficult to match with a simple circuit model. To illustrate this, Fig. 10 shows results for the CMC listed as MURATA PLA10AN2230R4D2B (22 mH) in Table III. From results in Fig. 10 it can be seen that in this case the CM response of the CMC is perfectly approximated but the DM curve has a slight deviation in the frequency of resonance with respect to the measured curve. In fact, a slight mismatch of DM curves at high frequencies can also observed in the DM curves of Fig. 7(b).

From the analysis of the previous results and also of the results obtained for all the CMCs in Table II, we can conclude that in general our method provides an accurate model of the CMC for a CM excitation (CM curve) and a good or fair approximation of the DM response of the CMC. To study the actual improvement provided by the high-frequency model obtained for the CMCs in prediction of the CM and DM noise emissions of a system, it is illustrative to measure the attenuation of a practical EMI filter mounting a CMC. To this end, we have constructed an EMI filter following a classical scheme with two thin-film *Y*-capacitors and

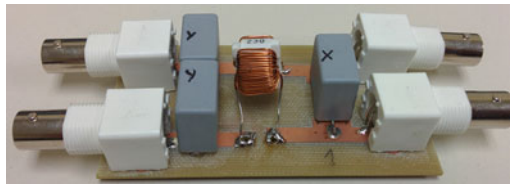

Fig. 11. EMI filter constructed with two 47nF-Cy-capacitors, one 470nF-Cx-capacitor and the CMC labeled as KEMET SC-02-30G in Table III.

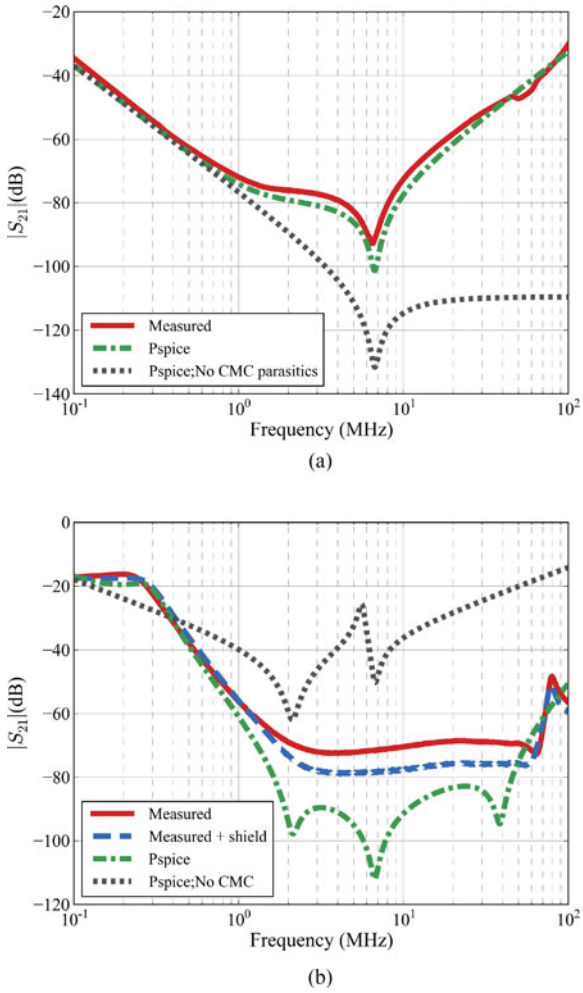

Fig. 12. Measured and approximated $|S_{21}|$ curves for the EMI filter shown and described in Fig. 11. (a) Common mode. (b) Differential mode.

one *X*-capacitor placed on both sides of a CMC [2], [4]. As for the CMC we have used the KEMET SC-02-30G model already analyzed in Fig. 7 and whose parasitic elements are shown in Table III. A picture of that filter is shown in Fig. 11. For this filter, we have measured the transmission coefficient $|S_{21}|$ for CM and DM noise. To this end, we have used the CM and DM connections of Fig. 2, where terminals labeled in that figure as 1 and 2 (input) correspond to the connectors shown at the left side of the filter in Fig. 11 and terminals labeled as 3 and 4 (output) correspond to connectors shown at the right side in Fig. 11. Results are shown in Fig. 12. In those graphs we have also included the $|S_{21}|$ curves provided by Pspice by using a circuit model of the filter that includes the equivalent series resistances

and equivalent series inductances of the capacitors. We have measured those parasitics obtaining approximately 12 nH and 40 mΩ for each capacitor [24]. The dotted curve in Fig. 12(a) corresponds to the attenuation of the CM noise predicted with this circuit model with no parasitic capacitance C_t included in the model of the CMC. It can be observed that above 1 MHz the predicted attenuation is much higher than that actually measured for the filter. However, by including the model of the CMC obtained with our method the $|S_{21}|$ curve provided by the circuit model matches the measured curve very closely . The measured and predicted attenuation of DM noise provided by the filter is shown in Fig. 12(b). The dotted line in Fig. 12(b) is obtained with a model of the filter that disregards the effect of the CMC. The two resonance peaks appearing in that curve are associated with the series *LC* resonances of the *Cx* and *Cy* capacitors. By comparing this curve with the two experimental curves included in the same figure, it is clear that the effect of the high-frequency parameters of the CMC cannot be ignored. In fact, Fig. 12(b) shows that when the leakage inductance $L - M$ and parasitic capacitances C_t and C_w of the CMC are included in the model of the filter the predicted attenuation of the DM is much closer to that actually measured. We have obtained similar results, both for the CM and DM attenuations, by substituting other CMCs in the same filter. It is interesting to note that in the DM case the coincidence between experimental and simulated data is not as close as that obtained for the CM curves of Fig. 12(a). This effect has been previously noticed by Tan *et al.* [16], and attributed to the effects of coupling between the capacitors and the CMC [25]. We have checked this by manually inserting two 5 cm $\times$ 5 cm squares of copper tape (not grounded) between the CMC and the capacitors. The measured curve in this configuration is represented by an additional line, labeled as measured + shield, in Fig. 12(b). That curve shows that the magnetic shielding provided by the metallic sheets causes the attenuation of the filter to increase by almost 10 dB in the 2–40 MHz frequency range, getting closer to the attenuation predicted by our circuit model, thus confirming that the mismatch between calculated an measured attenuation is due to the mentioned mutual coupling effect. It is appropriate to clarify that this effect is much weaker in the CM case due to the fact that the *Cx* capacitor is not active for CM excitation and also to the different spatial distribution of the stray magnetic fields created by the CMC under CM and DM excitations.

Summing up, results for the attenuation of a real EMI filter show that the high-frequency model of the CMC described above can greatly improve the accuracy in the prediction of performance of the filter. Also, they show that, at least for typical placement of components, DM noise is very sensitive to mutual coupling between components. In these conditions, the implementation of a more complex approach and circuit model to increase the accuracy of the model of the CMC for the DM noise could be ineffectual unless the impact of mutual couplings is also considered in the analysis [26]. Also, effects as capacitive coupling to filter chassis could have some impact on shielded filters.

Results analyzed so far show that in general the method proposed here provide a good approximation of the CM attenuation

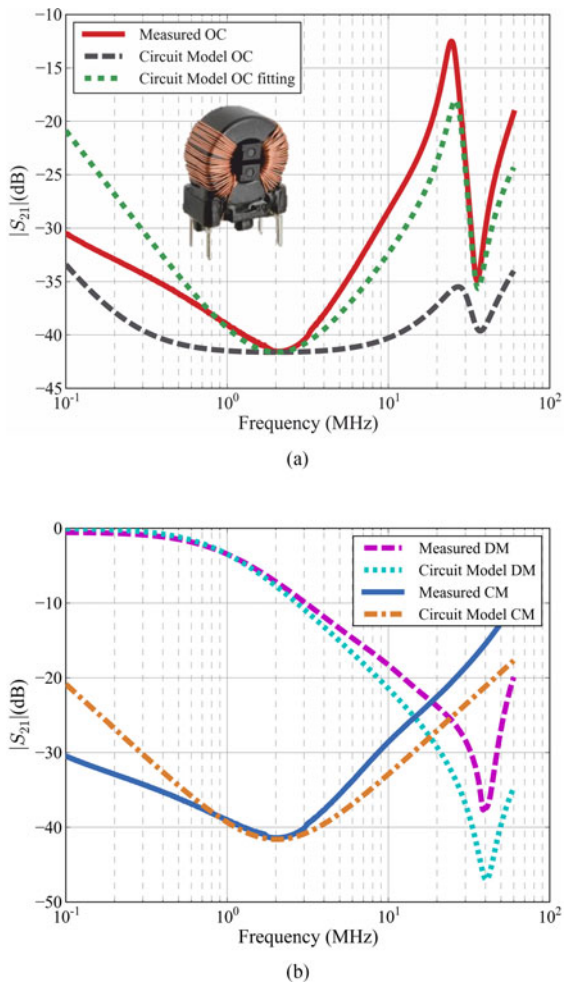

Fig. 13. Measured and approximated $|S_{21}|$ curves for the nanocrystalline CMC shown in the upper figure and listed as WÜRTH ELEKTRONIK 7448011008 (8 mH) in Table III. (a) Open circuit (OC). (b) Common mode (CM) and differential mode (DM).

of a CMC along with a good to fair approximation of the DM response of the CMC. This could be very useful to predict the actual performance of EMI filters, specially when the simplicity of the measurement technique and procedure for extraction of the parameters of the circuit model are considered. However, the method of characterization of CMCs proposed here can fail or provide only approximate results in some cases where the permeability of the core of the CMC presents a rapid rate of variation with frequency, as for example happens with nanocrystalline material [5], [12], [27]. For example, Fig. 13 shows the results obtained with a nanocrystalline CMC of 8 mH (WÜRTH ELEKTRONIK 7448011008 in Table III). The gray dashed line in Fig. 13(a) is the OC curve obtained by a circuit model whose parameters have been extracted departing from the measurements performed with an *LCR* meter following the alternative procedure described in Section III. Whereas for most CMCs analyzed this curve usually matches the measured curves very closely, in this case, however, it can be observed that the OC curve fails to approximate the measured OC curve. However, when the initial parameters are allowed to change by performing a curve-fitting of the measured curve, following the process

in Fig. 6, a better (although still not accurate) approximation is obtained. This is represented by the dotted line in Fig. 13(a). The parameters of Table III for this CMC correspond to this fitted curve. An inspection of these parameters, reveals that approximating the experimental OC curve requires a significant reduction of the the CM inductance ($L + M$) of the CMC with respect to the nominal value. This is explained by the abrupt decrease of the permeability of the core with the frequency commonly encountered in nanocrystalline materials [12], [27]. This rapid rate of variation of the permeability of the core causes that the CM and DM curves of this CMC can only be approximately fitted, as shown by Fig. 13(b). However, it is important to highlight that even in a case like this one, where an accurate circuit model of the CMC cannot be obtained with our method, the theoretical analysis presented here is still useful in the sense that it allows for a quick qualitative prediction of the expected performance of the CMC throughout the entire frequency range from a simple inspection of the measured OC curve. In case a more accurate circuit model of the CMC is required, this would make it necessary to try a more complex circuit model accompanied by a more complicated procedure of extraction of parameters [16], [17].

V. Conclusion

This paper investigates the response of a CMC to an excitation applied to one winding whereas the other winding is open circuited (OC connection). We present a modal analysis of the CMC that allows us to demonstrate that the response of the CMC when excited in this OC configuration conveys valuable information about both the CM and the DM attenuation provided by the CMC.

In this way, a quick measurement performed with a very simple setup makes it possible to anticipate the expected performance of a CMC both for CM and DM currents. This information can greatly speed up the design or redesign process of an EMI filter.

Moreover, the analysis presented in this paper provides analytical expressions for the transmission coefficients of the different connection configurations of the CMC and closed-form expressions for their frequencies of resonance. This permits the identification and calculation of the main parameters that determine the high-frequency behavior of a CMC. From these parameters, the expected attenuation provided by the CMC for both CM and DM currents can be readily obtained. Note that in contrast with methods requiring impedance (amplitude and phase) measurements by using several configurations, the method proposed here to characterize CMCs requires simple measurements, performed with simpler equipment (an SA with TG). Also, note that the measurement of frequencies of resonance is not affected by the attenuation and phase shift introduced by cables and connectors, therefore the careful calibration usually required to perform impedance measurements is not required.

The method presented here can be valuable tool in the sense that it allows, for example, to expedite the choice of the more appropriate CMC when several CMCs are available or to analyze the suitability of a particular CMC to suppress noise emissions that are above the limits in a certain frequency range. Note that this not necessarily require to construct a circuit model of the CMC. Moreover, by providing a method for readily estimating the parasitic that undermine the performance of a real CMC at high frequencies, this method allows the engineer to improve the accuracy of a circuit model intended to determine noise emissions of a power converter. In this sense, the characterization of the CMC is a particularly challenging and necessary step to obtain a complete model of the system.

The method has been validated by characterization and comparison of measured against predicted results for many different CMCs within an ample range of inductances and made up of different materials. From the analysis of those results, we conclude that in general the proposed method is able to provide a very good approximation for the CM response of the CMC and a good to fair approximation of the DM attenuation over a sufficiently wide frequency range. We have checked that the level of accuracy provided by the method allows one to effectively improve the high-frequency model of a typical EMI filter.

As for the limitations of the method, we have shown that, although the approach proposed here is designed to partially capture the intrinsic frequency-dependent behavior of the magnetic materials commonly used in CMCs, it can find it difficult to provide accurate high-frequency models of CMCs with cores showing an abrupt decrease of permeability with frequency, as it occurs for instance with some nanocrystalline materials. However, note that even for those difficult cases, the inspection of the OC curve in light of the theoretical analysis presented in this paper is still a valuable source of information to assess the expected performance of the CMC at high frequencies. Also, our method assumes that the CMC is perfectly symmetric. Despite this fact, it is interesting to note that the simple OC measurement described here could be employed to readily detect asymmetries of the CMC by measuring the attenuation provided by the CMC in the OC configuration from both windings.

Form the point of view of modeling of CMCs, the technique presented in this paper bridges the gap between simple modeling of CMCs from inductance provided by the datasheet and much more sophisticated approaches providing high-frequency models of CMCs. In contrast with our method, those methods are able to account for frequency-dependent inductances and, due to the use of more complex models for the CMC with a higher number of parasitic elements, in some cases higher-order resonances appearing for some CMCs above several tens of MHz can be incorporated into the model [17]. In return, those techniques require the following of much more complex and time-consuming processes involving many measurements with different connections of the CMC and/or the use of advanced numerical techniques. The results shown in this paper demonstrate that in many cases a sufficiently accurate model can be obtained with a much simpler technique.

References

[1] I. F. Kovacevic, T. Friedli, A. M. Musing, and J. W. Kolar, "3-D electromagnetic modeling of parasitics and mutual coupling in EMI filters," *IEEE Trans. Power Electron.*, vol. 29, no. 1, pp. 135–149, Jan. 2014.

[2] C. R. Paul, *Introduction to Electromagnetic Compatibility*. Hoboken, NJ, USA: Wiley, 2006.
[3] J. Brombach, M. Jordan, F. Grumm, and D. Schulz, "Converter topology analysis for aircraft application," in *Proc. Int. Symp. Power Electron. Elect. Drives, Autom. Motion*, Jun. 2012, pp. 446–451.
[4] L. Tihanyi, *Electromagnetic Compatibility in Power Electronics*. Oxford, U.K.: Newnes, 1995.
[5] A. V. d. Bossche and V. C. Valchev, *Inductors and Transformers for Power Electronics*. Boca Raton, FL, USA: CRC Press, 2005.
[6] M. Nave, "On modeling the common mode inductor," in *Proc. IEEE Int. Symp. Electromagn. Compat.*, 1991, pp. 452–457.
[7] S. Wang, F. C. Lee, and J. D. van Wyk, "Design of inductor winding capacitance cancellation for EMI suppression," *IEEE Trans. Power Electron.*, vol. 21, no. 6, pp. 1825–1832, Nov. 2006.
[8] R. Anne and F. Leferink, "Analysis of common mode inductors and optimization aspects," in *Electromagnetic Interference Issues in Power Electronics and Power Systems*, F. Zare, Ed. Emirate of Sharjah, United Arab Emirates: Bentham Science Publishers, Mar. 2011, ch. 1, pp. 3–37.
[9] W. G. Hurley and W. H. Wölfle, *Transformers and Inductors for Power Electronics: Theory, Design and Applications*. Hoboken, NJ, USA: Wiley, 2013.
[10] P. Okyere and E. Habiger, "A novel physically-based PSPICE-compatible-model for common-mode chokes," in *Proc. Int. Symp. Electromagn. Compat.*, 1999, pp. 33–36.
[11] A. Roc'h, H. Bergsma, D. Zhao, B. Ferreira, and F. Leferink, "A new behavioural model for performance evaluation of common mode chokes," in *Proc. 18th Int. Zurich Symp. Electromagn. Compat.*, 2007, pp. 501–504.
[12] M. Kovacic, Z. Hanic, S. Stipetic, S. Krishnamurthy, and D. Zarko, "Analytical wideband model of a common-mode choke," *IEEE Trans. Power Electron.*, vol. 27, no. 7, pp. 3173–3185, Jul. 2012.
[13] I. F. Kovacevic, T. Friedli, A. M. Muesing, and J. W. Kolar, "3-D electromagnetic modeling of EMI input filters," *IEEE Trans. Ind. Electron.*, vol. 61, no. 1, pp. 231–242, Jan. 2014.
[14] S. Skibin and I. Stevanovic, "Behavioral circuit modeling of chokes with multi-resonances using genetic algorithm," in *Proc. IEEE Int. Symp. Electromagn. Compat.*, 2011, pp. 454–458.
[15] J. L. Kotny, X. Margueron, and N. Idir, "High-frequency model of the coupled inductors used in EMI filters," *IEEE Trans. Power Electron.*, vol. 27, no. 6, pp. 2805–2812, Jun. 2012.
[16] W. Tan, C. Cuellar, X. Margueron, and N. Idir, "A high frequency equivalent circuit and parameter extraction procedure for common mode choke in the EMI filter," *IEEE Trans. Power Electron.*, vol. 28, no. 3, pp. 1157–1166, Mar. 2013.
[17] I. Stevanovic, S. Skibin, M. Masti, and M. Laitinen, "Behavioral modeling of chokes for EMI simulations in power electronics," *IEEE Trans. Power Electron.*, vol. 28, no. 2, pp. 695–705, Feb. 2013.
[18] L. O. Chua and Y. F. Lam, "A theory of algebraic n-ports," *IEEE Trans. Circuit Theory*, vol. 20, no. 4, pp. 370–382, Jul. 1973.
[19] J.-S. Hong, *Microstrip Filters for RF/Microwave Applications*. Hoboken, NJ, USA: Wiley, 2011.
[20] D. Marquardt, "An algorithm for least-squares estimation of nonlinear parameters," *J. Soc. Ind. Appl. Math.*, vol. 11, no. 2, pp. 431–441, 1963.
[21] *Industrial, Scientific, and Medical Equipment Radio-Frequency Disturbance Characteristics Limits and Methods of Measurement*, EN55011:2011/CISPR 11, 2009.
[22] *Information Technology Equipment—Radio Disturbance Characteristics—Limits and Methods of Measurement*, EN55022:2011/CISPR 22, 2008.
[23] *The FCC 47 CFR Part 15 From the Federal Communications Commission: Rules and regulations for EMC*, FCC Part 15.
[24] S. Wang, F. Lee, and W. Odendaal, "Cancellation of capacitor parasitic parameters for noise reduction application," *IEEE Trans. Power Electron.*, vol. 21, no. 4, pp. 1125–1132, Jul. 2006.
[25] S. Wang, F. Lee, D. Chen, and W. Odendaal, "Effects of parasitic parameters on EMI filter performance," *IEEE Trans. Power Electron.*, vol. 19, no. 3, pp. 869–877, May 2004.
[26] T. De-Oliveira, J.-L. Schanen, J.-M. Guichon, and L. Gerbaud, "Optimal stray magnetic couplings for EMC filters," *IEEE Trans. Ind. Appl.*, vol. 49, no. 4, pp. 1619–1627, Jul. 2013.
[27] R. Lebourgeois, S.Bérenguer, C. Ramiarinjaona, and T. Waeckerlé, "Analysis of the initial complex permeability versus frequency of soft nanocrystalline ribbons and derived composites," *J. Magn. Magn. Mater.*, vol. 254, pp. 191–194, 2003.

Authors' photographs and biographies not available at the time of publication.